



# Effect of temperature on light induced degradation in methylammonium lead iodide perovskite thin films and solar cells



Ghada Abdelmageed<sup>a,c</sup>, Cameron Mackeen<sup>b</sup>, Kaitlin Hellier<sup>b</sup>, Leila Jewell<sup>b</sup>, Lydia Seymour<sup>b</sup>, Mark Tingwald<sup>b</sup>, Frank Bridges<sup>b</sup>, Jin Z. Zhang<sup>a</sup>, Sue Carter<sup>b,\*</sup>

<sup>a</sup> Department of Chemistry and Biochemistry, University of California, Santa Cruz, California 95064, United States

<sup>b</sup> Department of Physics, University of California, Santa Cruz, California 95064, United States

<sup>c</sup> Department of Radiation Physics, National Center for Radiation Research and Technology (NCRRT), Atomic Energy Authority (AEA), Nasr City, Cairo, Egypt

## ARTICLE INFO

### Keywords:

Perovskite  
Methylammonium lead iodide  
EXAFS  
Stability  
Photovoltaics

## ABSTRACT

In this study we investigate the light and heat-induced degradation of methylammonium lead iodide (MAPbI<sub>3</sub>) perovskite films in an inert atmosphere to exclude the effect of oxygen and humidity. Films aged under solar intensities started to degrade above 75 °C, while films in the dark degraded at 95 °C. To investigate the temperature-induced degradation mechanism, spectroscopic techniques such as Ultraviolet-Visible (UV-Vis) absorption spectroscopy, X-Ray Diffraction (XRD), Extended X-ray Absorption Fine Structure (EXAFS), and Fourier Transform Infrared (FT-IR) were used. Results show that the films aged under light at 75 °C degraded to a mixture of PbI<sub>2</sub> and metallic Pb. In contrast, films aged thermally in the dark, or with light and oxygen, degraded to PbI<sub>2</sub> only. MAPbI<sub>3</sub> solar cells were aged to show the effect of the metallic lead on the charge transfer mechanism.

## 1. Introduction

Organometal halide perovskites (OMH-perovskite) with the structure ABX<sub>3</sub> (A = organic cation, B = metal cation, and X = halide anion) have unique properties such as a tunable band gap, easy fabrication process, high extinction coefficients, low recombination rate, high carrier mobility, and enhanced power conversion efficiency (PCE) up to 22.1%, indicating that OMH-perovskite has a great potential in photovoltaics applications [1–6]. However, the rapid instability of the material in the presence of environmental elements, such as light, oxygen, heat, and moisture, limits its application in industry [7–9]. Different types of environmental exposure can induce different degradation pathways, so it is important to examine the degradation of the OMH-perovskite samples under each condition to have a full assessment of the stability of the material. Many degradation studies have focused on oxygen and water, however both can be kept from interacting with the perovskite layer using proper encapsulation. However, solar cells are all subject to operation under light and elevated temperatures. To date, only a few studies have been done on the stability of OMH-perovskite films and solar cells with light in the absence of water [10–12]. Based on these studies, oxygen is critical in the light induced degradation of MAPbI<sub>3</sub> films, while in the absence of oxygen, the perovskite films were found to be stable. However, the stability of

perovskites under light at varying temperatures has not been fully addressed.

In this work, we examined the degradation of MAPbI<sub>3</sub> perovskite films and solar cells with light in an inert atmosphere at two different temperatures (55 °C and 75 °C). In addition, we evaluated the thermal stability of perovskite films in the dark at three temperatures (75 °C, 85 °C, and 95 °C) to have an accurate assessment of the thermal factor in the light degradation mechanism. Our data show the MAPbI<sub>3</sub> perovskite to be stable under intense light of approximately 360 mW/cm<sup>2</sup> at 55 °C, but under the same conditions at an elevated temperature of 75 °C, it degrades to a mixture of PbI<sub>2</sub> and metallic Pb. The influences of different degradation processes on the samples were investigated in detail.

## 2. Material and methods

The materials used in these experiments include N,N-dimethylformamide (DMF, spectroscopic grade, OmniSolv), 2-propanol (spectroscopic grade, Fisher Scientific), Lead iodide (PbI<sub>2</sub>, 99%, ACROS Organics, Fisher Scientific), and methylammonium iodide (MAI, Dyesol), TiO<sub>2</sub> nanoparticles (Solaronix), and Poly-3-hexylthiophene (P3HT, Sigma-Aldrich). All chemicals were used as received without any further purification. The methylammonium lead iodide (MAPbI<sub>3</sub>)

\* Corresponding author.

E-mail address: [sacarter@ucsc.edu](mailto:sacarter@ucsc.edu) (S. Carter).

films were prepared in air at humidity level of  $40\% \pm 2\%$  RH on cleaned borosilicate glass and quartz slides using a slightly modified two step method [13]. The films were prepared by spin coating  $50 \mu\text{l}$  of dissolved  $\text{PbI}_2$  in DMF (461 mg/ml) at 6000 rpm for 5 s, then dried at  $80^\circ\text{C}$  for 30 min in air.  $150 \mu\text{l}$  MAI solution (10 mg/ml in 2-propanol) was spin-coated on the films for 1 min at 0 rpm (loading time), then for 20 s at 3000 rpm to remove the excess. The films were dried again at  $80^\circ\text{C}$  for 30 min in air. This preparation method gives  $\text{MAPbI}_3$  thin films with thickness of  $\sim 250$  nm.  $\text{MAPbI}_3$  solar cell fabrication is detailed in the [Supplementary information](#).

The degradation process was induced by heating the samples with light using a mercury lamp (spectrum in [Fig. S1](#)), with illumination intensity of  $360 (\pm 10) \text{ mW/cm}^2$  (high intensity compared with  $100 \text{ mW/cm}^2$  AM1.5 solar light, though heavily weighted in the UV) in a nitrogen filled environment with very low oxygen and humidity levels ( $< 10$  ppm and  $< 0.1$  ppm, respectively). For samples characterized by temperature degradation without light, samples were placed on a hotplate and heated to the desired temperature in an  $\text{N}_2$  glovebox. Surface temperatures of the thin film were recorded over time, and are considered the temperature of the sample.

To facilitate the comparison of samples aged at different conditions, we will use the formula X-Y-Z to label the samples, where X is D (dark) or L (light) to indicate whether the sample was subjected to light or kept in the dark; Y is  $\text{N}_2$  or  $\text{O}_2$ , representing whether the sample was aged in nitrogen or dry air; and Z is the temperature of the sample substrate, in Celsius. For example, the sample label  $\text{D-N}_2-95$  represents the sample aged in a dark,  $\text{N}_2$  filled environment with a substrate temperature of  $95^\circ\text{C}$ , and the label  $\text{L-O}_2-22$  represents the sample aged in dry air at  $22^\circ\text{C}$  with light exposure. [Table \(S1\)](#) in [Supplementary information](#) provides the details of each sample according to its label.

The optical absorption spectra of the films were measured using a Jasco V-670 spectrophotometer. XRD analysis (XRD, Rigaku Americas Miniflex Plus powder diffractometer) was performed at a voltage of 40 kV and current of 44 mA, with a scanning angle range of  $10\text{--}60^\circ$  ( $2\theta$ ) with a rate of  $3^\circ/\text{min}$ . Fourier Transform Infrared (FT-IR) spectra were recorded with a Perkin Elmer Spectrum One FT-IR spectrophotometer using KBr pellets as substrates. The Pb  $L_{\text{III}}$  edge EXAFS data were collected at the Stanford Synchrotron Radiation Lightsource (SSRL) on beamline 4-1 using a Si (220) double monochromator, detuned 50% at 13,200 eV to reduce harmonics. The data were collected in fluorescence mode with a Ge multi-channel detector at a temperature of 8 K. Slit heights were approximately 0.4 mm, which gives an energy resolution of  $\sim 1.3$  eV. The data were reduced using standard techniques (RSXAP) [8], converted to  $k$ -space, and Fourier transformed to  $r$ -space. The Fourier transform range for all the samples is  $3.5\text{--}12.5 \text{ \AA}^{-1}$  with a window rounding of  $0.3 \text{ \AA}^{-1}$ .

### 3. Results and discussion

The light induced degradation of  $\text{MAPbI}_3$  perovskite films was examined in a dry,  $\text{N}_2$  environment to exclude the role of oxygen and to avoid the destructive effect of humidity. The stability of the perovskite films exposed to light of  $360 \pm 10 \text{ mW/cm}^2$  was monitored over the course of 4 days at two different temperatures ( $55^\circ\text{C} \pm 2^\circ\text{C}$  and  $75^\circ\text{C} \pm 2^\circ\text{C}$ ). The experimental setup is detailed and illustrated in the [Supplementary information](#). The perovskite films aged at  $55^\circ\text{C}$  were stable, showing no visible change; meanwhile, films aged at  $75^\circ\text{C}$  were visibly degraded. We found this interesting, as previous publications investigating light induced degradation of perovskite material in  $\text{N}_2$  atmosphere concluded that it had either a negligible or no sign of decomposition [10–12,27]. The film aged at the lower temperature is in agreement with those previous studies; however, the film aged at the higher temperature showed the opposite result, indicating an additional factor initiated this unanticipated decomposition. Furthermore, the degraded film had a unique gray-yellow color post degradation, which

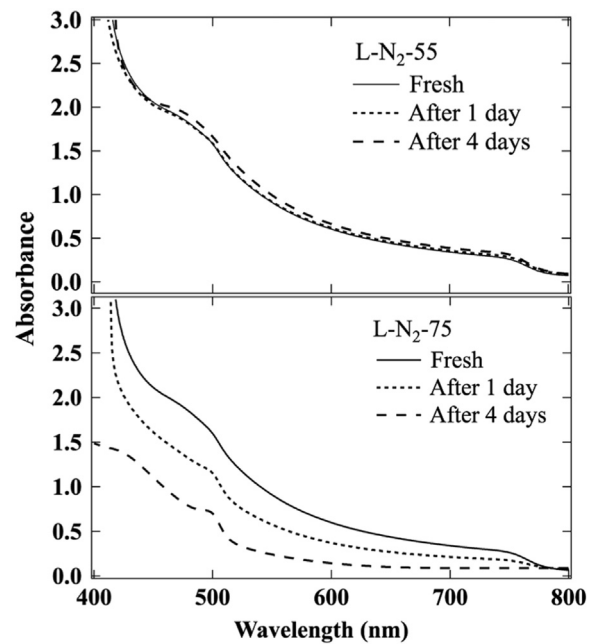


**Fig. 1.** The UV-Vis absorbance spectrum of  $\text{MAPbI}_3$  perovskite films aged with intense light in  $\text{N}_2$  filled environment in different positions. Top: the curves represent the perovskite film aged facing away from the lamp (face down) with temperature of  $55^\circ\text{C}$ . Bottom: the curves represent the perovskite film aged facing the lamp (face up) with temperature of  $75^\circ\text{C}$ .

is uncommon and does not resemble the bright yellow color of  $\text{PbI}_2$  films - the typical remnant material after  $\text{MAPbI}_3$  degradation. An image of the film before and after degradation process, compared with films aged in different setups, is shown in the [Supplementary information \(Fig. S3\)](#). By taking the UV-Visible absorbance spectra of the aged samples for 4 days of continuous illumination, as seen in [Fig. 1](#), we confirmed that only the sample exposed to light with elevated temperature was degraded and lost the signature perovskite onset at 790 nm that reflects the optical bandgap ( $E_g = 1.56$  eV) [14].

To understand the role of heat in the degradation process, the stability of  $\text{MAPbI}_3$  films were observed at different temperatures ( $75^\circ\text{C}$ ,  $85^\circ\text{C}$ , and  $95^\circ\text{C}$ ) without light exposure. The perovskite films were aged on a hotplate in a dark,  $\text{N}_2$  filled setup; their UV-Vis absorbance spectra are illustrated in [Fig. 2](#). It is clear that after 1 day the perovskite started to show slight degradation at  $85^\circ\text{C}$ , and showed almost complete degradation at  $95^\circ\text{C}$ . This result is in agreement with previous studies that reported thermal decomposition in  $\text{MAPbI}_3$  at  $85^\circ\text{C}$  in an inert atmosphere [15,16]. Meanwhile, the sample kept at  $75^\circ\text{C}$ , the same temperature as the degraded sample under light, did not show any sign of degradation. Therefore, it is likely that the intensity of the light added energetic effects to trigger degradation of the perovskite at  $75^\circ\text{C}$ .

To determine the degradation pathway, the changes in the perovskite structure aged under these various conditions were measured via XRD analysis, as shown in [Fig. 3](#). For comparison purposes,  $\text{MAPbI}_3$  films were prepared and aged under light in dry air at room temperature ( $22^\circ\text{C}$ ) using the same setup detailed in a previous paper [10]. It is well documented that  $\text{O}_2$  plays a crucial role in light induced degradation of perovskite, where free radicals such as superoxides are generated and subsequently interact with the organic cation of the perovskite molecule, which leads to degradation to  $\text{PbI}_2$  [10–12]. As shown in [Fig. 3](#), The fresh sample showed the expected diffraction peaks assigned to (110), (220), (310) and (330) at  $14.23^\circ$ ,  $28.47^\circ$ ,  $31.85^\circ$ , and  $43.08^\circ$  respectively, with lattice parameter values of  $a = 12.5 \text{ \AA}$ ,  $b = 26.6 \text{ \AA}$ , and  $c = 8.92 \text{ \AA}$  and  $\alpha = \beta = \gamma = 90^\circ$  that indicate an orthorhombic structure [17]. The XRD spectra of the degraded  $\text{MAPbI}_3$  films (light in dry air and in dark with high temperature

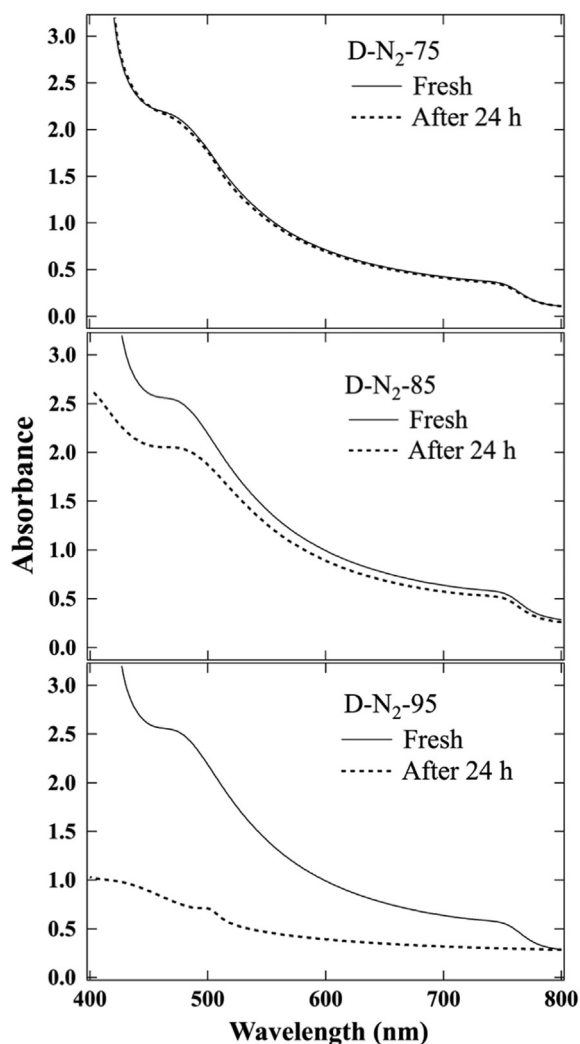


Fig. 2. UV-Vis absorbance spectra of MAPbI<sub>3</sub> perovskite films aged in dark in an N<sub>2</sub> filled environment, at three different temperatures (75 °C, 85 °C, and 95 °C).

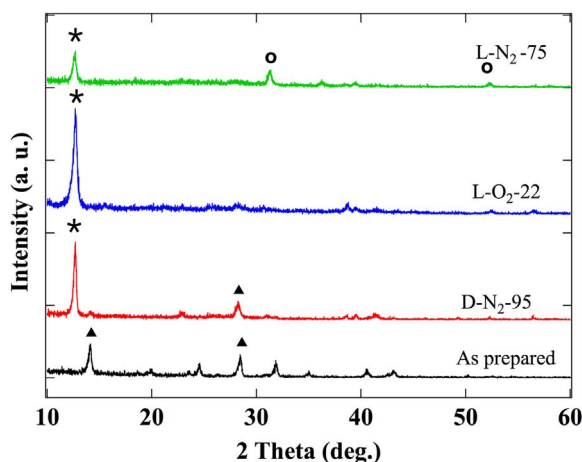


Fig. 3. X-ray diffraction (XRD) spectra of MAPbI<sub>3</sub> perovskite films in different conditions: as prepared (black), aged in dark at 95 °C (red), aged under light in dry air at room temperature ~ 30 °C (blue), and aged under light in N<sub>2</sub> filled environment at ~ 75 °C (green). PbI<sub>2</sub> peaks at 2θ = 12.5° are marked by asterisks; MAPbI<sub>3</sub> peaks at 2θ = 14.23°, 28.47° are marked by solid triangles; and metallic Pb peak at 2θ = 31.25° is marked by the open circle. (For interpretation of the references to color in this figure legend, the reader is referred to the web version of this article.)

(95 °C)) show only peaks that are assigned to hexagonal PbI<sub>2</sub> (2θ = 12.5°). Meanwhile, the film aged with light at 75 °C in inert atmosphere (face up) shows a mixed phase of hexagonal PbI<sub>2</sub> (2θ = 12.5°) and cubic metallic Pb (2θ = 31.25°, 52.23°) [27].

Degradation to metallic lead has previously been reported in a studies that involved aging perovskite in vacuum [27,28]. Li et al. investigated the degradation of MAPbI<sub>3</sub> films irradiated by a blue light laser (wavelength 408 nm) with intensity of about 7 times of AM1.5 in ultrahigh vacuum and conversion to metallic lead was noticed. The author concluded that the perovskite decomposed due to sensitivity to laser irradiation rather than heating effects of the laser [28]. Additionally, Tang et al. studied the photoinduced degradation of MAPbI<sub>3</sub> films at different environmental conditions including air, pure N<sub>2</sub> gas, and vacuum. The study confirmed that perovskite was stable under light in N<sub>2</sub> and metallic lead formation was only found in the samples degraded in vacuum. It was deduced that during photostress in vacuum, highly volatile methylammonium iodide is formed and lost, causing iodine vacancies that eventually reduced Pb<sup>2+</sup> to Pb<sup>0</sup> [27]. However, since our results show metallic lead formation in an N<sub>2</sub> environment contrary to both of these studies, we conclude that more studies are needed to fully understand the different mechanisms of degradation.

To further evaluate the Pb metal degradation pathway, extended x-ray absorption fine structure (EXAFS) analysis of the Pb L<sub>III</sub> absorption edge was conducted. The region starting ~30 eV above the absorption edge is the EXAFS region where the X-ray absorption oscillates with energy. A background subtraction is carried out to remove contributions from other atoms; this isolates the absorption step and the oscillatory region. Above the absorption edge,

$$\mu = \mu_0(1 + \chi) \quad (1)$$

where  $\mu_0$  is a slowly varying function, and  $\chi$  is the EXAFS function. By extracting  $\chi$ , the local crystal structure can be probed. This entails removing the slowly varying function,  $\mu_0$ , converting from energy to  $k$ -space and performing a fast Fourier transform of  $k^2\chi(k)$ . The resulting function in real space ( $r$ -space) has peaks corresponding to each shell of neighboring atoms. For the Pb L<sub>III</sub> data the transform window is 3.5–12.5 Å<sup>-1</sup>, where:

$$\chi(k) = \frac{\mu_{\text{edge}}(E)}{\mu_0(E)} - 1 \quad (2)$$

The EXAFS function,  $\chi(k)$ , can also be calculated for known crystal structures using FEFF7 [18]. More importantly, the contribution for each individual pair distribution, corresponding to a neighboring shell of atoms, can be calculated; when transformed to  $r$ -space each function has a peak at a well-defined distance. These individual standards are summed to fit the real-space data using the RSXAP package [19].

The EXAFS data are shown in Fig. 4 for three samples aged under different conditions; the top panel shows data for the sample degraded under light exposure where the temperature of the film was 75 °C (L-N<sub>2</sub>-75). This film is the only one with a significant fraction of Pb metal present. The other two samples (aged in dark at 95 °C – D-N<sub>2</sub>-95 – and with light at room temperature – L-O<sub>2</sub>-22) show only the Pb-I first neighbor peak below 4 Å. The data above 4.5 Å for the sample aged in the dark at 95 °C (not shown) shows the presence of the Pb-Pb peak from PbI<sub>2</sub>, indicative of the formation of PbI<sub>2</sub> as described in previous work [10]. These data were fit over the range 2.8–4.0 Å to a sum of two FEFF7 generated peaks: a Pb-I peak from a MAPbI<sub>3</sub> structure and a Pb-Pb peak from simple Pb metal. For the sample exposed to light in N<sub>2</sub> with a film temperature of 75 °C (L-N<sub>2</sub>-75), the fit yields a non-negligible contribution from the Pb-Pb peak generated from a cubic lead crystal. For this sample, the resulting aged film contains 39.5% metallic lead. Alternatively, if the same data are fit using a linear combination of previously acquired MAPbI<sub>3</sub>, PbI<sub>2</sub> and metallic Pb data, we again obtain the same fraction – 39.5% metallic Pb. Goodness of fit is better for the fit with theoretical standards (see Table S2 in Supplementary

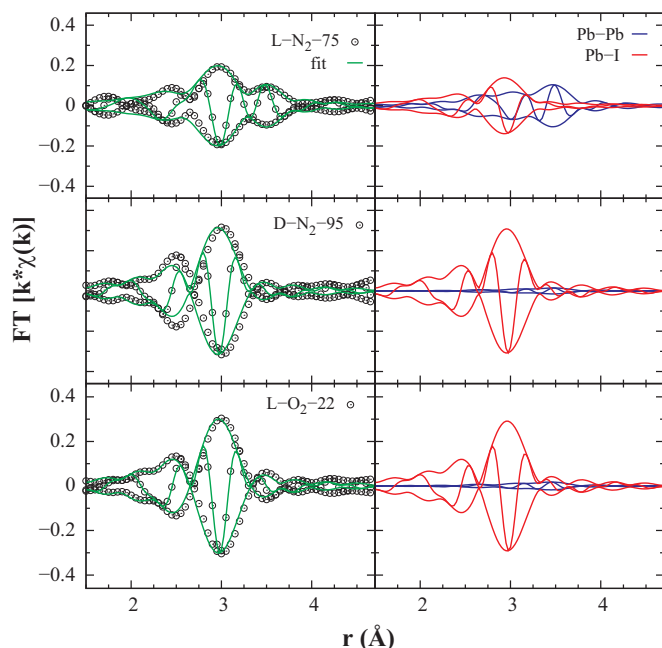


**Fig. 4.** Left: Real-space EXAFS data for samples aged under different conditions (circles) and the fit (green line). Right: Peaks (components) for each fit. These fits use FEFF7 generated standards and show the difference between the sample exposed to light in  $N_2$  at  $T = 75^\circ C$  and the other samples. The fit of the former requires a nearly equal combination of a Pb-I (perovskite) peak (red) and a Pb-Pb (metallic Pb) peak (blue) near  $3.5 \text{ \AA}$ , compared with almost no Pb-Pb contribution from Pb metal in the other two samples. (For interpretation of the references to color in this figure legend, the reader is referred to the web version of this article.)

#### information).

In contrast, fits of the  $r$ -space data for a sample kept in the dark at  $95^\circ C$  (D- $N_2$ -95) and a sample exposed to light and dry air at room temperature (L- $O_2$ -22) had a negligible contribution from this metallic Pb-Pb peak. The  $r$ -space data differ between the sample exposed to light in  $N_2$  with a temperature of  $75^\circ C$  and the other samples near  $\sim 3.5 \text{ \AA}$  and  $6 \text{ \AA}$ . From Fig. 5, it is evident that the prominent peak positions for the metallic Pb data occur at these distances.

To analyze the change in the molecular structure of the organic component of the perovskite films, FT-IR was performed before and after degradation for the sample exposed to light at  $75^\circ C$  (Fig. 6a) and the sample in the dark at  $95^\circ C$  (Fig. 6b). As demonstrated in Fig. 6, the characteristic vibrational bands of methylammonium are identified. The bands are assigned to  $CH_3$  rocking at  $910 \text{ cm}^{-1}$ ; C-H scissoring at  $1470 \text{ cm}^{-1}$  for the  $CH_3$  functional group; N-H wagging at  $660 \text{ cm}^{-1}$ ;  $NH_3$  rocking at  $947, 961, 1252$ ;  $NH_3$  scissoring at  $1654 \text{ cm}^{-1}$ ; and N-H stretching at  $3208 \text{ cm}^{-1}$  for the  $NH_3$  functional group [20–22]. In the case of the sample degrading via the combined effect of light and heat (Fig. 6a), it is clear that the ammonium bands, especially at  $660 \text{ cm}^{-1}$ ,  $947 \text{ cm}^{-1}$ , and  $1654 \text{ cm}^{-1}$ , have decreased significantly in intensity compared to the methyl bands. This result indicates that the concentration of  $NH_3$  functional groups in the sample is declining at a higher rate than the concentration of  $CH_3$ . This may be due to a deprotonation process that converts the ammonium molecules to amines, or some other mechanism that requires the loss of  $NH_3$  molecules. In Fig. 6b, the FT-IR spectra of the film degraded by heat alone also shows a decrease in the ammonium bands, which indicates that the NH bonds are the weakest link in the perovskite structure. In a previous investigation, the thermal degradation of  $MAPbI_3$  was studied, and  $NH_3$  and  $CH_3I$  gases were observed by using thermal analytical techniques such as thermal gravimetric analysis (TGA) and differential thermal analysis (DTA) coupled with a mass spectrometer [3]. The proposed degradation mechanism is seen in Eq. (3). Since the boiling points of  $NH_3$  and  $CH_3I$  are  $-33.34^\circ C$  and  $42.43^\circ C$  respectively, the ammonium

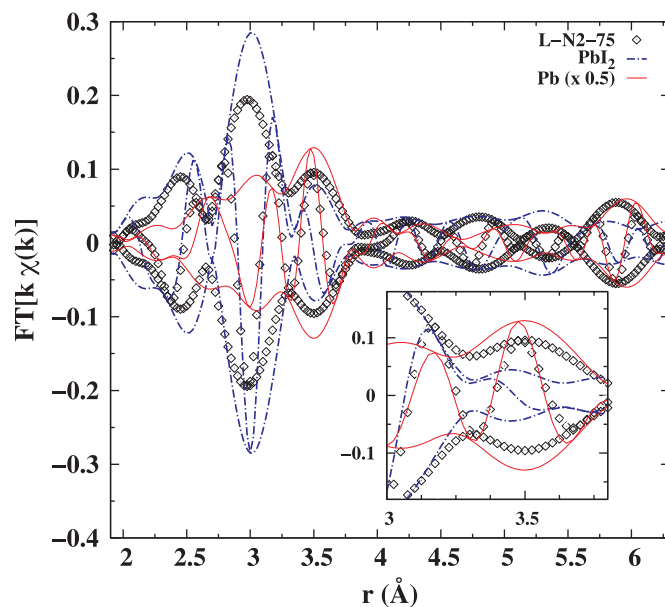


**Fig. 5.** Real-space EXAFS data overlaid to show the phase matching ( $Re\{\chi\}$ ) of metallic Pb (red line) to the data collected for the sample exposed to light in  $N_2$  at  $75^\circ C$  (black diamonds). The dashed blue line is  $PbI_2$  data which is the expected product of perovskite degradation. There is a clear phase mismatch in the region at  $\sim 3.5 \text{ \AA}$ , as seen in the magnified inset. The metallic Pb data (reference data collected in 1994) are scaled by 0.5 just to make the amplitude comparable. The EXAFS  $r$ -space data (L- $N_2$ -75) in the other region of interest, near  $\sim 6 \text{ \AA}$ , also match well with the peak seen in metallic Pb data.

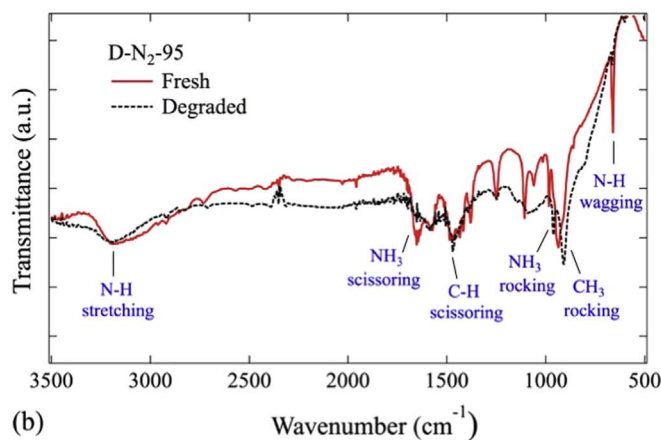
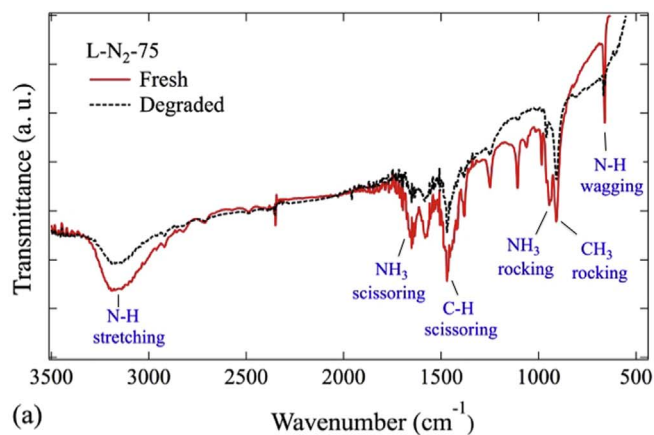


**Fig. 6.** FT-IR spectra of  $MAPbI_3$  samples degraded by different initiators in an  $N_2$  environment. FT-IR spectra of  $MAPbI_3$  film before and after degradation (a) under light at  $75^\circ C$  and (b) at  $95^\circ C$  in dark.



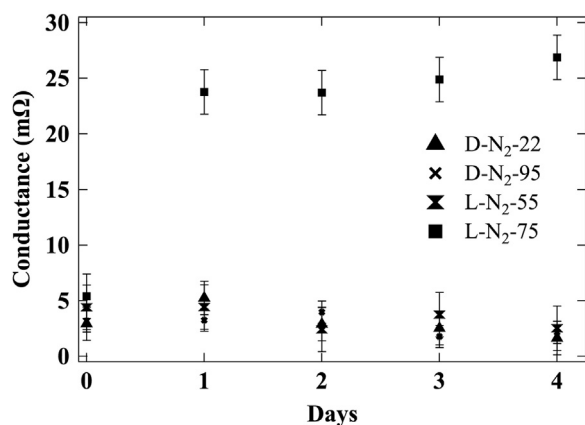
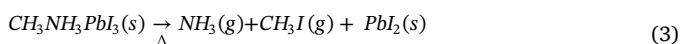
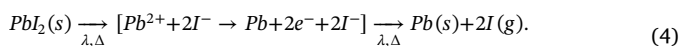


Fig. 7. Conductance values at 1 V applied voltage of MAPbI<sub>3</sub> solar cells aged for 4 days in N<sub>2</sub> atmosphere under different conditions – dark at room temperature (22 °C), dark at 95 °C, light at 55 °C, and light at 75 °C.

molecule leaves the structure at a higher rate than the methyl iodide [23,24]. This may explain the greater decrease in N-H bands compared to the C-H bands in Fig. 6b.



However, in the case of degradation with light at 75 °C, the solid resultant product of the mixture of metallic lead and lead iodide might be attributed to the weak nature of the iodine bonds that can break and lead to iodine sublimation under the photothermal stress [25]. Therefore, the degradation mechanism induced by both light and heat could be initiated with the breakage of the iodide bonds. To further investigate our proposal, we prepared a lead iodide film (using the first step of the two steps method mentioned in the experimental section) and aged it under direct light in N<sub>2</sub> at 75 °C and noticed the color transformation from bright yellow to gray, indicating the loss of iodine and converting a large portion of it to metallic lead. We confirmed the change in structure by taking XRD before and after degradation (Fig. S5). This would seem to indicate the breakdown of the MAPbI<sub>3</sub> to PbI<sub>2</sub>, followed by photodissociation of the Pb-I bonds resulting in neutral lead and iodine atoms:



It would seem reasonable to assume that the elevated temperature of the sample provides a drop in the photodissociation energy of the PbI<sub>2</sub> molecule, hence allowing the breakdown under the same light levels of samples above a certain temperature.

To evaluate the impact of the degradation pathway on the device performance, MAPbI<sub>3</sub> solar cells were fabricated and aged in an inert atmosphere under the following conditions: dark at room temperature, dark at 95 °C, light at 55 °C, and light at 75 °C. The device fabrication and aging processes, the solar cell parameters, and JV curves are detailed in the Supplementary information. Fig. S7 shows the normalized values of the solar cell parameters of the aged devices ( $J_{sc}$ ,  $V_{oc}$ , FF, and PCE). The devices kept in dark at room temperature and under light at 55 °C did not suffer a loss in their efficiency or a significant change in their parameters. Devices kept in dark at 95 °C after 1 day had an initial drop (~23%) in the values of  $V_{oc}$  (from 0.89 to 0.69 V), which is in agreement of reported  $V_{oc}$  values of MAPbI<sub>3</sub> and PbI<sub>2</sub> solar cells respectively [26], confirming the degradation of MAPbI<sub>3</sub> to PbI<sub>2</sub>. The  $V_{oc}$  values remained at the same level for the rest of the degradation process indicating that PbI<sub>2</sub> was the final degradation product of the active layer. Meanwhile, in the device degraded under light at 75 °C, the  $V_{oc}$  continued to drop over time, reaching ~75% of its initial value. The rapid decrease in  $V_{oc}$  is due to the formation of lead, which leads to shunting paths through the device. Another indicator of lead formation

is the conductance (G) values of the aged devices. In Fig. 7, the evolution of conductance values at applied voltage of 1 V of the aged solar cells is illustrated. This shows that the conductance of the sample aged at 75 °C under light rapidly increased to over 5 times its initial value, which is expected to be due to the transition of portions of the MAPbI<sub>3</sub> to Pb metal. The other aging conditions do not show a significant increase in conductance values, which suggest no lead metal was forming in these samples.

#### 4. Conclusion

In summary, we report on the degradation of MAPbI<sub>3</sub> films and solar cells in an N<sub>2</sub> environment with light and found that temperature plays a crucial role in the degradation mechanism. The film degraded under light at a temperature of 75 °C contained both metallic Pb and PbI<sub>2</sub>, in contrast to the thermal degradation of the film in the dark beginning at 85 °C resulting in only PbI<sub>2</sub>. This indicates two separate degradation pathways – the former due to a combination of thermal and photo dissociation, and the latter due to only thermal dissociation, with very different resultant products.

While the role of high temperatures has been shown to break down the MAPbI<sub>3</sub> perovskite to the PbI<sub>2</sub> precursor, we show the importance of the light interaction in the breakdown temperature, and the additional negative effects of light resulting in the formation of metallic lead. This has strong implications for the future role of perovskites in solar applications, especially in current interests in multijunction cells and in solar concentrators. By understanding this breakdown, the correct preventative measures can be taken to keep the perovskite active layer from decaying to even worse conditions than excess lead iodide in the system.

Further work must be done to understand the temperature/light relationship and energies involved in the iodine-lead dissociation, and addition of electrical load to an active perovskite cell under light with elevated temperature. However, recognizing the resultant films brings us a step closer to making perovskites a competitive player in the thin film photovoltaic industry.

#### Acknowledgement

This work was supported and partially funded by Cultural Affairs and Mission Sector in Egypt and by the Bay Area Photovoltaic Consortium, DOE prime award DE-EE0004946 and subaward 60965033-51077. The XRD experiments were performed by J. Hauser and A. Durand at the UC Santa Cruz X-ray Facility, supervised by S. Oliver and funded by the NSF DMR-1126845. JZZ is grateful to support from NASA and UCSC Special Research Fund for financial support. SAC acknowledges support from NSF CHE 1710652. The EXAFS experiments were performed at the Stanford Synchrotron Radiation Lightsource (SSRL), which is supported by the U.S. Department of Energy, Office of Science, Office of Basic Energy Sciences, under Contract No. DE-AC02-76SF00515.

#### Appendix A. Supporting information

Supplementary data associated with this article can be found in the online version at <http://dx.doi.org/10.1016/j.solmat.2017.09.053>.

#### References

- [1] A. Kojima, K. Teshima, Y. Shirai, T. Miyasaka, Organometal halide perovskites as visible-light sensitizers for photo-voltaic cells, *J. Am. Chem. Soc.* 131 (2009) 6050–6051.
- [2] C. Wehrenfennig, G.E. Eperon, M. Johnston, H. Snaith, L.M. Herz, High charge carrier mobilities and lifetimes in organolead trihalide perovskites, *Adv. Mater.* 26 (2014) 1584–1589.
- [3] C.S. Ponseca Jr., T. Savenije, M. Abdellah, K. Zheng, A. Yartsev, T. Pascher, T. Harlang, P. Chabera, T. Pullerits, A. Stepanov, J.-P. Wolf, V. Sundstrom,

- Organometal halide perovskite solar cell materials rationalized: ultrafast charge generation, high and microsecond-long balanced mobilities, and slow recombination, *J. Am. Chem. Soc.* 136 (2014) 5189–5192.
- [4] C. Wehrenfennig, M. Liu, H. Snaith, M.B. Johnston, L.M. Herz, Charge-carrier dynamics in vapour-deposited films of the organolead halide perovskite  $\text{CH}_3\text{NH}_3\text{PbI}_3$ , *Energy Environ. Sci.* 7 (2014) 2269–2275.
- [5] N.-G. Park, Crystal growth engineering for high efficiency perovskite solar cells, *Cryst Eng Comm.* 18 (2016) 5977–5985.
- [6] M.M. Lee, J. Teuscher, T. Miyasaka, T.N. Murakami, H.J. Snaith, Efficient hybrid solar cells based on meso-superstructured organometal halide perovskites, *Science* 338 (2012) 643–647.
- [7] G. Niu, X. Guo, L. Wang, Review of recent progress in chemical stability of perovskite solar cell, *J. Mater. Chem. A* 3 (2015) 8970–8980.
- [8] T. Leijtens, G.E. Eperon, S. Pathak, A. Abate, M.M. Lee, H.J. Snaith, Overcoming ultraviolet light instability of sensitized  $\text{TiO}_2$  with meso-superstructured organometal tri-halide perovskite solar cells, *Nat. Commun.* 4 (2013) 2885.
- [9] G. Niu, W. Li, F. Meng, L. Wang, H. Dong, Y. Qiu, J. Study on the stability of  $\text{CH}_3\text{NH}_3\text{PbI}_3$  films and the effect of post-modification by aluminum oxide in all-solid-state hybrid solar cells, *Mater. Chem. A* 2 (2014) 705–710.
- [10] G. Abdelmageed, L. Jewell, K. Hellier, L. Seymour, B. Luo, F. Bridges, J.Z. Zhang, S. Carter, Mechanisms for light induced degradation in  $\text{MAPbI}_3$  perovskite thin films and solar cells, *Appl. Phys. Lett.* 109 (2016) 233905.
- [11] N. Aristidou, I. Sanchez-Molina, T. Chotchuangchutchaval, M. Brown, L. Martinez, T. Rath, S.A. Haque, The role of oxygen in the degradation of methylammonium lead trihalide perovskite photoactive layers, *Angew. Chem. Int. Ed.* 54 (2015) 8208–8212.
- [12] D. Bryant, N. Aristidou, S. Pont, I. Sanchez-Molina, T. Chotchuangchutchaval, S. Wheeler, James R. Durrant, S.A. Haque, Light and oxygen induced degradation limits the operational stability of methylammonium lead triiodide perovskite solar cells, *Energy Environ. Sci.* 9 (2016) 1850–1850.
- [13] H. Ko, J. Lee, N. Park, 15.76% efficiency perovskite solar cell prepared under high relative humidity: importance of  $\text{PbI}_2$  morphology in two-step deposition of  $\text{CH}_3\text{NH}_3\text{PbI}_3$ , *J. Mater. Chem. A* 3 (2015) 8808–8815.
- [14] N.A. Manshor, Q. Wali, K.K. Wong, S.K. Muzakir, A. Fakharuddin, L. Schmidt-Mende, R. Jose, Humidity versus photo-stability of metal halide perovskite films in a polymer matrix, *Phys. Chem. Chem. Phys.* 18 (2016) 21629–21639.
- [15] E.J. Juarez-Perez, Z. Hawash, S.R. Raga, L.K. Ono, Y. Qi, Thermal degradation of  $\text{CH}_3\text{NH}_3\text{PbI}_3$  perovskite into  $\text{NH}_3$  and  $\text{CH}_3\text{I}$  gases observed by coupled thermogravimetry mass spectrometry analysis, *Energy Environ. Sci.* 9 (2016) 3406–3410.
- [16] B. Conings, J. Drijkoningen, N. Gauquelin, A. Babayigit, J. D'Haen, L. D'Olieslaeger, A. Ethirajan, J. Verbeeck, J. Manca, E. Mosconi, F. De Angelis, H.-G. Boyen, Intrinsic thermal instability of methylammonium lead trihalide perovskite, *Adv. Energy Mater.* 5 (2015) 150047.
- [17] C.-W. Chen, H.-W. Kang, S.-Y. Hsiao, P.-F. Yang, K.-M. Chiang, H.-W. Lin, Efficient and uniform planar-type perovskite solar cells by simple sequential vacuum deposition, *Adv. Mater.* 26 (38) (2014) 6647–6652.
- [18] A.L. Ankudinov, J.J. Rehr, Relativistic calculations of spin-dependent x-ray-absorption spectra, *Phys. Rev. B* 56 (1997) R1712 (R).
- [19] C.H. Booth. R-Space X-ray Absorption Package. See: <<http://lise.lbl.gov/RXSAP/>>, 2010.
- [20] N.J. Jeon, J.H. Noh, Y.C. Kim, W.S. Yang, S. Ryu, S. Il Seok, Solvent engineering for high-performance inorganic–organic hybrid perovskite solar cells, *Nat. Mater.* 13 (2014) 897–903.
- [21] A. Cabana, C. Sandorfy, The infrared spectra of solid methylammonium halides, *Spectrochim. Acta* 18 (1962) 843–861.
- [22] T. Glaser, C. Müller, M. Sendner, C. Krekeler, O.E. Semonin, T.D. Hull, O. Yaffe, J.S. Owen, W. Kowalsky, A. Pucci, R. Lovrinčić, Infrared spectroscopic study of vibrational modes in methylammonium lead halide perovskites, *J. Phys. Chem. Lett.* 6 (2015) 2913–2918.
- [23] R. Overstreet, W.F. Giauque, Ammonia. The heat capacity and vapor pressure of solid and liquid, heat of vaporization. the entropy values from thermal and spectroscopic data, *J. Am. Chem. Soc.* 59 (2) (1937) 254–259.
- [24] A.P. Kudchadker, S.A. Kudchadker, R.P. Shukla, P.R. Patnaik, Vapor pressures and boiling points of selected halomethanes, *J. Phys. Chem. Ref. Data* 8 (1979) 499.
- [25] P.H. Svensson, L. Kloo, Synthesis, structure, and bonding in polyiodide and metal iodide–iodine systems, *Chem. Rev.* 103 (5) (2003) 1649–1684.
- [26] D.H. Cao, C.C. Stoumpos, C.D. Malliakas, M.J. Katz, O.K. Farha, J.T. Hupp, M.G. Kanatzidis, Remnant  $\text{PbI}_2$ , an unforeseen necessity in high-efficiency hybrid perovskite-based solar cells, *APL Mater.* 2 (2014) 091101.
- [27] X. Tang, M. Brandl, B. May, I. Levchuk, Y. Hou, M. Richter, H. Chen, S. Chen, S. Kahmann, A. Osvet, F. Maier, H.-P. Steinruck, R. Hock, B.G.J. Matt, C.J. Brabec, Photoinduced degradation of methylammonium lead triiodide perovskite semiconductors, *J. Mater. Chem. A* 4 (2016) 15896–15903.
- [28] Y. Li, X. Xu, C. Wang, B. Ecker, J. Yang, J. Huang, Y. Gao, Light-induced degradation of  $\text{CH}_3\text{NH}_3\text{PbI}_3$  hybrid perovskite thin film, *J. Phys. Chem. C* 121 (7) (2017) 3904–3910.